Enhanced Photorefractivity from Ion-Doped Polymer-Dispersed Liquid Crystals

Jeffrey E. Hall and Daniel A. Higgins*

Department of Chemistry, Kansas State University, Manhattan, Kansas 66506

Received: June 21, 2004; In Final Form: August 11, 2004

Dynamic near-field scanning optical microscopy (NSOM) and asymmetric two-beam coupling experiments are performed on thin films of photorefractive polymer-dispersed liquid crystals (PDLCs). Results obtained from films doped with perylene (serving as the photoexcitable electron donor) and *N*,*N*′-dioctyl-1,4,5,8-naphthalene diimide (NDI) (the electron acceptor) are compared to those obtained from films that have also been doped with tetrabutylammonium tetrafluoroborate (TBATFB). Both the dynamic NSOM and two-beam coupling results provide clear evidence for enhanced photorefractivity in films doped with permanent ions such as TBATFB. Computer simulations of the NSOM results lend supporting evidence and also provide valuable information on the origins of this enhancement. It is concluded that the enhanced optical response arises from the nonlinear dependence of the liquid crystal orientation state on the electric fields within individual liquid crystal droplets and, hence, the concentrations of both permanent and photogenerated ions. These observations suggest a possible alternative means for enhancing the response of photorefractive devices employing dye-doped polymer-dispersed liquid crystals.

Introduction

Dye-doped liquid crystals possess several unique attributes that make them potentially useful as photorefractive materials.[1−5] Generally, they exhibit larger photorefractive gain coefficients than other organic and inorganic photorefractives,[6] allowing for the development of thin-film optical devices. Enhanced photorefractivity in liquid crystal systems results from their strong birefringence and the ease by which they can be reoriented by small electric fields. In addition, these and other organic photorefractives can potentially be made into flexible or moldable devices. One of the primary shortcomings of bulk liquid crystal photorefractives, however, is their limited resolution. Liquid crystals tend to respond collectively to both externally applied and locally generated electric fields. As a result, it is difficult to induce large changes in the refractive index over short distance scales in liquid crystalline phases.

The use of dye-doped polymer-dispersed liquid crystals (PDLCs) has recently been proposed as a means to overcome this resolution limit.[7] In PDLCs, the liquid crystalline phase is divided into small noninteracting domains that are separated from each other by a polymer matrix. The liquid crystal domains frequently take the form of spheroidal or ellipsoidal droplets. Unfortunately, increased field strengths are required to induce photorefractivity in dye-doped PDLCs. In addition, the photorefractive gain coefficient is reduced in proportion to the volume fraction of liquid crystal present.

A number of researchers have recently sought to improve the photorefractive gain of PDLC-based devices by a number of different methods. These include the use of donor and acceptor molecules that are more efficient at generating charge carriers[1,8] and the development of materials that are more effective at trapping either photogenerated cations or anions.[9] Liquid crystals with greater birefringence could also be employed. Finally, as in all photorefractive materials, the gain coefficient can also be optimized by minimizing the dark conductivity of the material.[10] In many instances this is accomplished by scrupulous elimination of all permanent, mobile ions.

In this paper, we conclusively show that, unlike other photorefractive materials,[11] the photorefractive response of dye-doped PDLCs is actually enhanced by the purposeful addition of permanent ions to the liquid crystalline phase. This method was originally tested as a means to enhance the weak optical signals in near-field scanning optical microscopy (NSOM) studies of these materials.[12,13] Predictions of NSOM signal enhancement were obtained from ongoing theoretical simulations.[12,13] Here, it is shown that the inclusion of permanent ions in the liquid crystal droplets enhances both the dynamic NSOM signals and the beam coupling ratio in bulk asymmetric two-beam coupling studies of similar samples. Such effects have not previously been described and indeed run counter to previously developed knowledge on other photorefractive materials.[14,15] It is concluded that the enhancements observed herein are likely a result of the unique properties of photorefractive PDLCs, for which the addition of permanent ions does not lead to a significant increase in dark conductivity. Rather, the added ions substantially increase the strength of space-charge fields that develop within the droplets. They also increase the rate at which these fields form and decay. The nonlinear dependence of the liquid crystal alignment on field strength in PDLCs then leads to enhanced NSOM signals and ultimately to enhanced photorefractivity.

Experimental Section

Materials. Photorefractive PDLC thin films were prepared from dye-doped liquid crystal and an aqueous solution of poly(vinyl alcohol) (PVA). The liquid crystal employed (E7) was purchased from Merck and was used as received. PVA (9000 M_w, 80% hydrolyzed) was purchased from Aldrich and was purified by dialysis against several portions of ultrapure water (18 MΩ cm). Perylene dye was obtained from Aldrich and was used as received. *N*,*N*′-Dioctyl-1,4,5,8-naphthalene diimide

* Corresponding author. E-mail: higgins@ksu.edu.

10.1021/jp047302y CCC: $27.50
Published on Web 09/17/2004

(NDI) was synthesized as described previously[16] and purified by column chromatography. The two dyes were incorporated into the liquid crystal by first dissolving them in a small amount of chloroform and then adding the chloroform solution to the liquid crystal. The chloroform was allowed to evaporate by letting the solution stand overnight. The final concentrations of perylene and NDI in the liquid crystal were 2.3 and 7.0 mM, respectively. Ion-doped samples were prepared in a similar manner by adding a chloroform solution of tetrabutylammonium tetrafluoroborate (TBATFB) to the dye-doped liquid crystal. Liquid crystal solutions with ion concentrations ranging from 0 to approximately 40 μM were employed.

PDLC samples for NSOM experiments were prepared by emulsifying the dye-doped liquid crystal in a 3 wt % aqueous PVA solution to yield a 3 wt % liquid crystal suspension. A few drops of this emulsion were then spin-cast onto a clean indium tin oxide (ITO)-coated (20 Ω/cm^2) glass microscope slide, and the solvent was allowed to evaporate. The films were dried at room temperature overnight prior to use.

Samples for two-beam coupling experiments were prepared in a similar manner. Here, a 20 wt % aqueous liquid crystal emulsion was employed. Photorefractive devices were prepared by placing a 20 μm thick Mylar spacer onto an ITO-coated slide. A drop of the aqueous emulsion was placed in the center of a hole cut into the spacer, and the solvent was then allowed to evaporate. A second ITO-coated slide was then placed on top of the film and spacer. Finally, the sandwich device was clamped and cemented together using super glue.

Methods. All near-field optical birefringence and topographic images were recorded in raster-scan fashion on a modified Veeco Metrology Aurora NSOM. This instrument has been described previously.[17] Aluminum-coated NSOM fiber probes were produced in house. Tip−sample separation was maintained at approximately 5 nm by tuning-fork-detected shear-force feedback.[18]

For both static and dynamic NSOM birefringence imaging, 633 nm light from a HeNe laser was coupled into the NSOM probe fiber. Broadband half-wave and quarter-wave plates were used to set the polarization state (linear) of the 633 nm light emerging from the probe tip. A polarization purity of greater than 90% was measured in the far field for each tip employed. Light transmitted through the sample was collected using a 0.8 numerical aperture objective and was detected using a photomultiplier tube (PMT). A polarization analyzer was placed in front of the PMT and was set to pass light polarized perpendicular to that emerging from the NSOM probe.

Electric-field-induced dynamics were studied using methods described previously,[13] in the same microscope. Briefly, a modulated electric field was applied between the aluminum-coated NSOM probe and the ITO-coated substrate using a standard digital waveform generator. Electrical connections were made to the NSOM probe and the substrate using silver paint and fine transformer wire. A sinusoidally modulated (100−400 Hz) waveform was employed.

Electron transfer between perylene and NDI was initiated by coupling 488 nm light from an argon ion laser into the NSOM probe fiber, simultaneously with the 633 nm light used to monitor the birefringent state of the liquid crystal. Typically, $\approx$150 μW of 633 nm light and $\approx$200 μW of 488 nm light were coupled into the fiber, yielding $\approx$50−100 pW of elliptically polarized light at 488 nm from the NSOM probe aperture. Residual 488 nm light transmitted through the sample and collected by the objective was blocked using a holographic notch filter and a dichroic mirror.

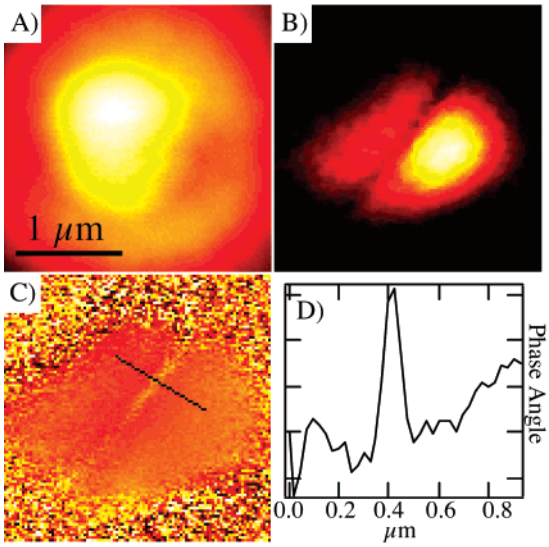

Figure 1. Dynamic NSOM images of a photorefractive PDLC droplet: (A) topography, (B) amplitude, and (C) phase images. (D) Line profile of the phase angle represented by the line in (C).

The modulated PMT signal resulting from field-driven reorientation of the liquid crystal (as detected using 633 nm light) was fed into a lock-in amplifier. The amplitude and phase outputs from the lock-in at the second harmonic of the field modulation frequency were used to record dynamic NSOM images of the sample. Images were recorded before, during, and after photogeneration of ions.

Asymmetric two-beam coupling experiments were performed using experimental methods described previously in detail.[19] Briefly, p-polarized light at 488 nm from an argon ion laser was divided into two beams of similar power (9.7 and 5.2 mW) using a nonpolarizing beam splitter cube. These two beams were gently focused into vertically mounted photorefractive PDLC sandwich devices prepared as described above. The bisecting angle between the two beams was 1°, and the sample normal was rotated away from the beam axis by 35°, yielding an intensity grating in the sample with 9.2 μm periodicity. An optical chopper was mounted in one of the two beam paths. This beam was arbitrarily designated as the "pump beam"; the other is referred to below as the "probe beam". The optical power in each beam, after passage through the sample, was monitored using standard photodiodes.

An electric field was applied across the sample using a digital waveform generator and a high-voltage amplifier. The applied field consisted of both a dc component, as required to observe photorefractivity,[6,20] and an ac component to maintain the liquid crystal alignment, absent the dc field.[19] Asymmetric beam coupling was verified by using a lock-in amplifier to measure the amplitude of the probe beam modulation induced by chopping the pump beam at 500 Hz. The beam-coupling ratio was determined for several field strengths ranging from 0 to approximately 3 V/μm. A small background from pump beam light scattered onto the probe beam detector was subtracted from the data.

Results and Discussion

Electric-field-induced liquid crystal reorientation and ion-migration dynamics within individual dye-doped liquid crystal droplets were studied using NSOM methods described previously.[13] Topography, amplitude, and phase images (all simultaneously recorded) of a representative dye-doped PDLC droplet are shown in Figure 1. These images were obtained in the

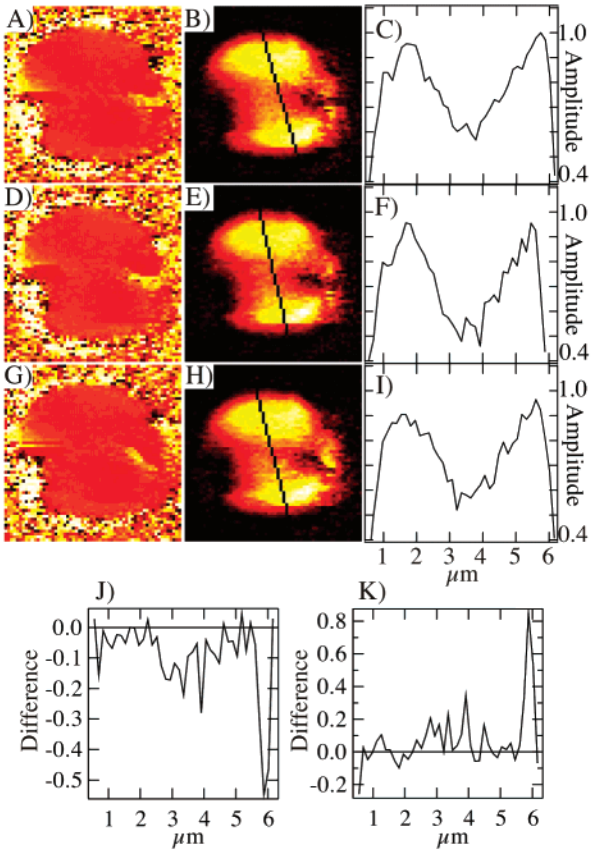

Figure 2. Dynamic NSOM images of an ≈6 μm diameter dye-doped liquid crystal droplet in the absence of permanent ions: (A) phase image and (B) amplitude image obtained using 633 nm light; (C) line profile from image (B); (D) phase image and (E) amplitude image of the same droplet, imaged during photogeneration of ions using 488 nm light; (F) line profile from image (E); (G) phase image and (H) amplitude image after photogeneration of ions; (I) line profile from image (H); (J) difference between line profiles taken before and during ion generation, relative to the line profile obtained before ion generation; (K) difference between the line profiles taken during and after ion generation, relative to the line profile obtained during ion generation.

absence of photogenerated ions. The liquid crystal within most such droplets is organized in the so-called "bipolar" configuration.[21] Clear differences between dynamics in the bulk of this droplet and in the equatorial plane (oriented perpendicular to the film) are observed.[21] The equatorial plane appears as a dark line (smaller signal amplitude) running through the center of the droplet in the amplitude image and a corresponding bright line (smaller phase lag) in the phase image. A line profile plotted across this region (see Figure 1D) demonstrates that sub-diffraction-limited (≈100 nm) optical resolution is obtained. The dynamics in the equatorial regions of bipolar droplets are complicated, but the observed phenomenon can generally be attributed to weaker field−molecule interactions and a greater elastic restoring force near the equatorial plane. Such effects have been explored previously in detail and are reflective of inherent spatial variations in the liquid crystal dynamics alone (i.e., they do not reflect spatial variations in ion dynamics).[21,22] Nevertheless, such spatial variations in the droplet's physical parameters do play an important role in governing the liquid crystal dynamics associated with photorefractivity.

Ion Generation and Liquid Crystal Dynamics in Dye-Doped PDLCs. The influence of photogenerated ions on the observed droplet dynamics was explored by recording dynamics images before, during, and after ion generation. Again, ion generation occurs by transfer of an electron from perylene to NDI, following perylene excitation using 488 nm light. Figure 2 presents typical dynamic NSOM images obtained from dye-doped PDLC droplets in the absence of purposefully added permanent ions. In all such images, 633 nm light was used to monitor the time-dependent, field-induced changes in the liquid crystal orientation state. The particular droplet shown in Figure 2 has a diameter of ≈6 μm. It does not show the same contrast along the equatorial plane as in Figure 1, perhaps because of imperfections in the liquid crystal organization or the tilting of its polar axis out of the sample plane. Such differences are representative of droplet-to-droplet variations commonly observed in these materials.

Figure 2A presents the phase image obtained from this droplet prior to ion generation. The mean phase angle measured in the central region of this droplet was defined as 0.0 ± 0.6°. The error bars reported on the phase angle (±0.6°) reflect the 95% confidence interval about the mean. All subsequent changes in the phase angle were defined relative to this image. Figure 2D shows the phase image obtained during photogeneration of ions. The mean phase angle measured in this image increased by 2° during ion generation. This change in phase angle is small but significant and indicates that the liquid crystal dynamics have become faster with an increase in the concentration of ions.[23] Finally, Figure 2G presents the phase image recorded after photogeneration of ions. Approximately 10 min had elapsed between the recording of the individual line scans in Figure 2D,G. In Figure 2G, the mean phase angle returned to 0.6° (±0.6°), consistent with recombination (or removal by some other mechanism) of the majority of photogenerated ions.

The amplitude images presented in Figure 2B,E,H provide complementary information on the changes in liquid crystal dynamics that occur during and after ion generation. To more clearly depict these changes, line profiles taken from these images are also plotted in Figure 2C,F,I (taken from Figure 2B,E,H, respectively). These line profiles were arbitrarily selected to pass through the center of the droplet. They have been offset slightly between images to compensate for image drift. The behavior observed in these line profiles is representative of the behavior throughout the droplet, as depicted in the images. Finally, plots of the differences between the line profiles obtained before and during ion generation (Figure 2J) and during and after ion generation (Figure 2K) are also given. Figure 2J was obtained by subtracting the line profile data in Figure 2C,F and dividing by that in Figure 2C. Figure 2K was generated in an identical fashion from Figure 2F,I.

A small reduction in the signal amplitude was observed throughout the droplet during ion generation. However, the amplitude reduction was most pronounced over the center of the droplet, where the amplitude decreased by ≈16% (see Figure 2J). This reduction in signal amplitude arises from cancellation of the externally applied field by the space-charge field formed within the droplet as a result of ion generation. The resulting internal field is smaller, and hence, the liquid crystal is not reoriented to the same degree. After ion generation, the amplitude signal returned to near its initial value, with the greatest increase in signal amplitude again occurring over the center of the droplet (see Figure 2K). As noted previously,[13] such spatial variations likely arise from the geometrical properties of the droplet. The photogenerated ions are expected to migrate to the highest and lowest points in the droplet, nearest the electrode (ITO-coated slide and aluminum-coated NSOM probe) surfaces. Hence, ions generated in outer circumferential

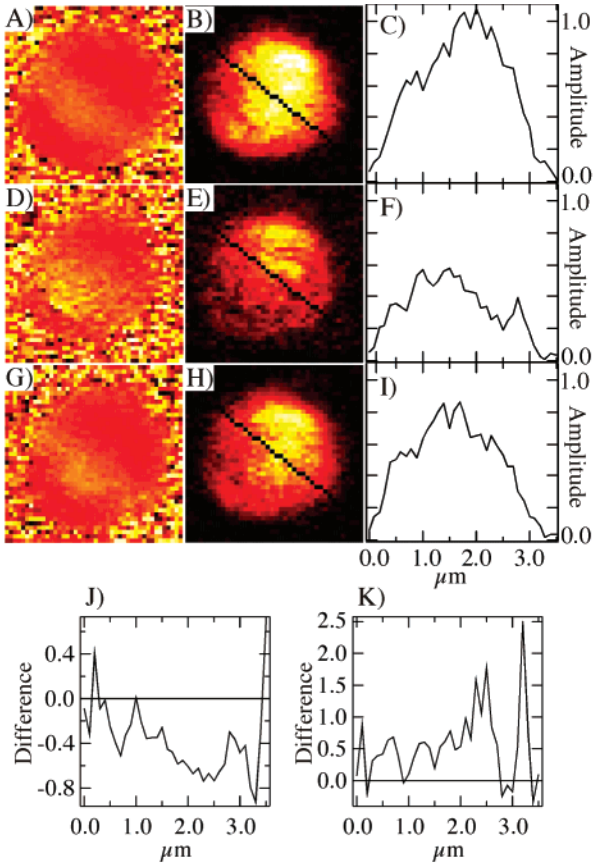

Figure 3. Dynamic NSOM images of an ≈3 μm diameter droplet doped with dye and 11 μM TBATFB: (A) phase image and (B) amplitude image obtained using 633 nm light; (C) line profile from image (B); (D) phase image and (E) amplitude image of the same droplet imaged during photogeneration of ions using 488 nm light; (F) line profile from image (E); (G) phase image and (H) amplitude image after photogeneration of ions; (I) line profile from image (H); (J) difference between line profiles taken before and during ion generation, relative to the line profile obtained before ion generation; (K) difference between the line profiles taken during and after ion generation, relative to the line profile obtained during ion generation.

droplet regions migrate toward the center of the droplet, causing the greatest change in field strength in this region.

It should be noted that neither the phase signal nor the amplitude signal recorded after ion generation returned to their original (pre-ion generation) values. These changes in signal, and hence liquid crystal dynamics, appear to be permanent, as deduced from numerous studies performed on different droplets over a period of several hours. Such changes are attributable to the generation of long-lived or permanent ions in these materials.

Dynamics in Ion-Doped and Dye-Doped PDLCs. The changes in the phase and amplitude signals described above are relatively small, although they are significant. In an effort to enhance these signals and to possibly obtain better images of spatial variations in the dynamics within individual droplets, studies of samples doped with TBATFB (in addition to perylene and NDI) were also conducted. TBATFB served to produce permanent ions when dissolved in the liquid crystal. The presence of these ions indeed enhances both the NSOM dynamics signals and photorefractivity in these materials (see below).

Figure 3 illustrates dynamic NSOM images obtained from a representative droplet containing 11 μM TBATFB. This droplet is ≈3 μm in diameter. The phase image shown in Figure 3A was recorded before photogeneration of ions. The mean phase angle in this image was set to 0 ± 2°. Again, the error bars reported represent the 95% confidence interval. Parts D and G of Figure 3 present phase images recorded during and after ion generation, respectively. During ion generation, the phase angle increased by 19 ± 3°, a much larger increase relative to the noise level than was observed in the absence of TBATFB. Experiments performed on several different droplets in both samples prove this is a general trend. Hence, it may be concluded that dissolved permanent ions lead to increased NSOM signal changes during ion generation. After ion generation, the phase angle returned to 2 ± 2°, once again indicating that most (but not all) of the photogenerated ions recombine or are removed.

The amplitude images shown in Figure 3 further demonstrate the enhancement of the NSOM signals in the presence of permanent ions. These images, taken before, during, and after ion generation, are shown in Figure 3B,E,H. Line profiles taken from these images are reported in Figure 3C,F,I, and differences between these line profiles are shown in Figure 3J,K. The line profiles most clearly demonstrate the magnitude of the changes in signal amplitude observed from this droplet. As in Figure 2, the line profiles were arbitrarily selected to be representative of the behavior observed in the images. A decrease in the signal amplitude during ion generation can be seen throughout the droplet but is especially pronounced in the droplet center, where the amplitude decreased by ≈60%. In general, the magnitude of the amplitude change over the entire line profile of an ion-doped droplet is much larger than that which occurs in the absence of permanent ions (i.e., TBATFB). Once again, the amplitude signal does not completely recover to its initial level after ion generation, indicating long-lived ions are still generated.

Modeling of the Effect of Permanent Ions. Several possible mechanisms exist by which the added permanent ions could enhance the observed changes in the NSOM signals. First, it is known that ionic species can stabilize the charge-separated radical ions produced in photochemical electron-transfer reactions.[24,25] The permanent ions help prevent back electron transfer, increasing the lifetimes of the photogenerated ions and, hence, their average concentrations. Second, the permanent ions may cause a change in the diffusion coefficients of either the cationic or anionic products, potentially resulting in larger space-charge fields.[11] It is likely that both of these mechanisms play some role. However, a third possible explanation also exists for the liquid crystalline materials studied here. Specifically, since the alignment of the liquid crystal depends nonlinearly on the local electric field strength, it is also possible that a small change in the concentration of ions (permanent or photogenerated), which leads to a small change in the local field strength, could lead to a much larger change in the orientation state of the liquid crystal. Although the nonlinear dependence of liquid crystal alignment on the field strength is well-known, to our knowledge the effect of permanent ions on these local fields and the resulting liquid crystal orientation have not been explored.

Here, computer simulations were performed in order to better understand the contributions of this latter mechanism to the observed TBATFB-dependent enhancement of the NSOM signals. The mathematical methods employed have been described previously.[13] Briefly, one-dimensional simulations of the dynamics associated with ion migration, space-charge field formation, and liquid crystal reorientation were performed using finite difference time domain (FDTD) methods to solve the necessary differential equations.[26] In each simulation, the sample was exposed to a sinusoidally modulated, externally applied

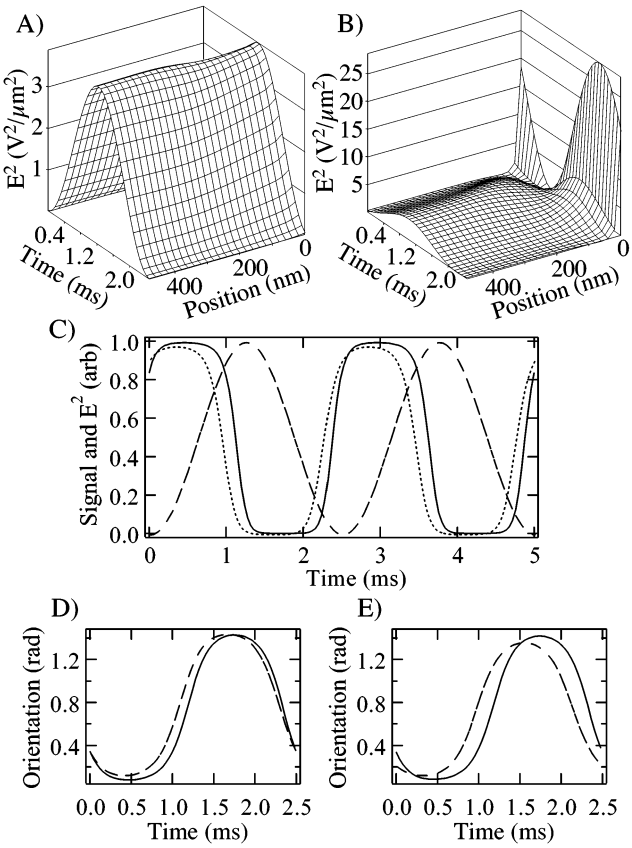

Figure 4. Squared electric field in a droplet with (A**)** 1 μM ions and (B**)** 30 μM ions as a function of time and position within the droplet. Position within the droplet is given as a function of distance from the polymer/liquid crystal interface at 0.0 nm. (C) Simulations of the optical signal as a function of time within an ion-doped liquid crystal droplet. Shown are data for ion concentrations of 30 μM ions (dotted line) and 1 μM ions (solid line), along with the applied, squared electric field (dashed line). (D) Liquid crystal orientation angle at the polymer/liquid crystal interface and (E) at the center of the droplet as a function of time resulting from the electric fields shown in (A**)** and (B). Dashed line: results for 30 μM ions. Solid line: results for 1 μM ions. These data were obtained after 13 field cycles in simulations using a 200 Hz modulated field.

electric field, exactly as in the experiments described above. The field modulation frequency in each simulation was also similar to that used in the NSOM experiments (i.e., 100−400 Hz). The number of ions employed in each simulation was held constant, simulating steady-state conditions. The initial concentration of ions is defined for each simulation described below and is meant to indicate the number of ions present in each droplet.

Figure 4 gives the results from a representative set of simulations, performed for a field modulation frequency of 200 Hz. Figure 4A depicts the squared electric field within a droplet containing 1 μM ions. The squared field is plotted with respect to time and position within the droplet, relative to the polymer/liquid crystal interface (at 0.0 nm). The electric field in the droplet remains relatively uniform throughout and has a relatively small magnitude ($\approx$2 V/μm at its peak). Figure 4B illustrates the squared electric field in a droplet containing 30 μM ions. In this case, the electric field within the droplet shows dramatic spatial and temporal variations. The field in the central regions of the droplet peaks below 2 V/μm (somewhat smaller than for 1 μM ions) while the field at the interface peaks at $\approx$5.3 V/μm a little later in time. These variations arise from the buildup and decay of a space-charge field at the polymer/liquid crystal interface. It is noteworthy that the differences observed between the results of these two simulations are due entirely to a change in ion concentration. All other parameters were identical.

The results obtained from these simulations were used to model the time-dependent liquid crystal orientation and the optical signal obtained in the NSOM experiments. Figure 4C shows plots of the optical signals derived from the two simulations discussed above. The simulated optical signals were calculated as previously described[27] and closely resemble those observed on an oscilloscope in actual NSOM experiments.[28] In fact, the two ion concentrations employed (1 and 30 μM) were selected specifically because they yielded model signals that closely mimicked those obtained experimentally. Hence, the ion concentrations in the real experiments are likely of similar magnitudes.

As shown in Figure 4C, the modulated optical signal shifts earlier in time (i.e., there is a smaller phase lag) as the ion concentration increases. Simultaneously, a decrease in the signal amplitude also occurs. These observations are identical to what is observed in the NSOM experiments (see Figures 2 and 3). The origins of these optical signals can be better understood by looking at the liquid crystal orientation at different positions within the droplet. Parts D and E of Figure 4 show the liquid crystal orientation as a function of time at the droplet surface and in the center of the droplet, respectively. In these plots, an orientation angle of 0.0 corresponds to the fully relaxed (zero-field orientation) of the liquid crystal and $\pi/2$ corresponds to fully field-aligned liquid crystal. Clearly, the liquid crystal reorientation process in the center of the droplet changes much more dramatically with a change in ion concentration (at least in this concentration range) than it does in the interfacial region. The modulated liquid crystal orientation in the droplet center is more strongly dampened at the higher ion concentrations because of the more rapid decay of the electric field within the droplet under these conditions. Hence, most of the changes in the NSOM signals observed in Figures 2 and 3 can be attributed to changes in the liquid crystal reorientation process deep within the droplets. Likewise, it may be concluded that the photorefractive effect in dye-doped PDLCs arises primarily from liquid crystal relaxation in these same droplet regions.

The origins of the enhanced NSOM signals observed at higher permanent ion concentrations are best demonstrated by determining the change in signal amplitude (or phase) induced by a small change in the ion concentration, for a series of ion concentrations. To this end, simulations of the change in the optical signal induced by a constant change in ion concentration of 2 μM for average ion concentrations of 20, 25, 30, 35, 40, 45, and 50 μM were performed. These simulations were performed at field modulation frequencies of 100, 200, and 400 Hz. Figure 5 plots log(dA/dC) vs log(C) obtained from these simulations. As is readily apparent from Figure 5, the change in amplitude for a small change in ion concentration (dA/dC) increases with increasing average ion concentrations at all simulated frequencies. That is, the simulations show that changes in the NSOM signals can be enhanced by adding permanent ions to the droplets, exactly as was observed in the NSOM experiments described above. At 100 Hz, the change in amplitude exhibits close to a cubic dependence on the average ion concentration while at 200 and 400 Hz the change is nearly linear in concentration.

Permanent Ions and Photorefractivity. The experimental and simulated results presented above prove that changes in NSOM signals obtained before and during ion generation can

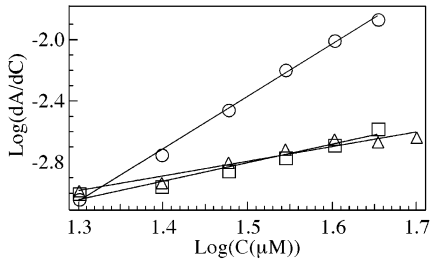

Figure 5. A log−log plot of the simulated change in amplitude (d*A*) for a small change in concentration (d*C*) vs the average ion concentration (*C*). These data were obtained for field modulation frequencies of 100 Hz (circles), 200 Hz (squares), and 400 Hz (triangles) after 13 field cycles in the simulations. Lines fit to these data yielded slopes of 3.4, 1.2, and 1.0 for 100, 200, and 400 Hz modulated fields, respectively.

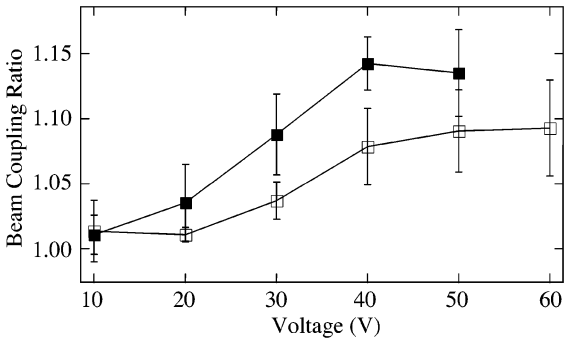

Figure 6. Results from asymmetric two-beam coupling experiments. Shown are the beam coupling ratios as a function of applied voltage for a pure, dye-doped PR-PDLC sample (open squares) and a PR-PDLC sample doped with 38 μM TBATFB (filled squares). The error bars represent the 90% confidence interval.

be enhanced by adding permanent ions to the liquid crystal droplets. They also suggest that addition of such permanent ions might lead to enhanced photorefractivity in dye-doped PDLC thin films. Asymmetric two-beam coupling experiments were conducted to explore this hypothesis.[19] In these experiments, the probe beam gain was measured as a function of applied voltage. Figure 6 presents these results as the beam coupling ratio, I(probe)/I_0(probe), where I_0(probe) is the probe beam signal absent the pump beam, but in the presence of the index grating I(probe) is the signal in the presence of the pump beam. These data reflect the average photorefractive response observed in multiple experiments performed on several replicate samples. The results clearly indicate that inclusion of permanent ions significantly enhances the photorefractive effect in bulk dye-doped PDLCs materials.

The enhancement of photorefractivity by the inclusion of permanent ions appears counterintuitive at first glance. It is well-known that the internal space-charge field within bulk photorefractive systems is adversely affected by an increase in the dark conductivity of the materials.[10,11] The inclusion of permanent ions such as has been done here would normally increase the dark conductivity and hence reduce the strength of the space-charge field and the strength of the photorefractive response. It is concluded that dye-doped PDLCs represent a special case in which addition of permanent ions to the liquid crystalline phase actually does not increase the dark conductivity significantly. The ions are encapsulated within the liquid crystal droplets, meaning they can only migrate to the polymer/liquid crystal interface and seldom reach the electrode surfaces. As a result, the ions are trapped within the liquid crystal droplets and aid in the buildup and decay of the space-charge field, without increasing the dark conductivity. Since both the liquid crystal reorientation process and the change in refractive index depend on the square of the electric field, the addition of permanent ions leads to an enhancement of the photorefractive effect in these materials.

Conclusions

In conclusion, NSOM experiments, computer simulations, and asymmetric two-beam coupling studies have proven that addition of permanent ions in the form of TBATFB to the dye-doped liquid crystalline phase of photorefractive PDLCs enhances both the NSOM dynamics signals and the photorefractive response of these materials. These observations run counter to previously developed models, which indicate the photorefractive effect should decrease as the dark conductivity of the material increases (i.e., by addition of permanent ions). It was concluded that addition of ions to PDLCs does not appreciably increase their dark conductivity but does enhance the rates of space-charge field formation and decay as well as the strength of these fields. It was also noted that the addition of ions likely enhances the stability of the photogenerated radical cations and anions and may also alter their diffusion coefficients. Overall, the results presented herein suggest that the inclusion of permanent ions may be useful as a means to increase the photorefractive response of dye-doped PDLCs.

Acknowledgment. This work was supported by the National Science Foundation (CHE-0092225).

References and Notes

(1) Wiederrecht, G.; Yoon, B.; Wasielewski, M. *Science* **1995**, *270*, 1794.
(2) Golemme, A.; Kippelen, B.; Peyghambarian, N. *Appl. Phys. Lett.* **1998**, *73*, 2408.
(3) Cipparrone, G.; Mazzulla, A.; Simoni, F. *Opt. Lett.* **1998**, *23*, 1505.
(4) Ono, H.; Kawatsuki, N. *Rec. Res. Dev. Appl. Phys.* **1998**, 47.
(5) Khoo, I. C.; Guenther, B. D.; Wood, M. V.; Chen, P.; Shih, M.-Y. *Opt. Lett.* **1997**, *22*, 1229.
(6) Zilker, S. *Chem. Phys. Chem.* **2000**, *1*, 72.
(7) Golemme, A.; Kippelen, B.; Maldonado, J.; Peyghambarian, N. *Proc. SPIE* **1998**, *3297*, 28.
(8) Khoo, I. C.; Slussarenko, S.; Guenther, B. D.; Shih, M.-Y.; Chen, P.; Wood, M. V. *Opt. Lett.* **1998**, *23*, 253.
(9) Wiederrecht, G.; Wasielewski, M. *J. Non. Opt. Phys. Mater.* **1999**, *8*, 107.
(10) Rudenko, E. V.; Sukhov, A. V. *JETP Lett.* **1994**, *59*, 142.
(11) Wiederrecht, G. Dynamic Holography in Photorefractive Liquid Crystals. In *Molecular and Supramolecular Photochemistry*; Schanze, K., Ramamurthy, V., Eds.; Marcel Dekker: New York, 2001; p 319.
(12) Hall, J. E.; Higgins, D. A. *ACS Symp. Ser.*, in press.
(13) Hall, J. E.; Higgins, D. A. *J. Phys. Chem. B* **2003**, *107*, 14211.
(14) Wiederrecht, G.; Wasielewski, M. *J. Am. Chem. Soc.* **1998**, *120*, 3231.
(15) Khoo, I. C. *IEEE J. Quantum Electron.* **1996**, 32.
(16) Wiederrecht, G.; Svec, W.; Niemczyk, M.; Wasielewski, M. *J. Phys. Chem.* **1995**, *99*, 8918.
(17) Hall, J. E.; Higgins, D. A. *Polym. Mater. Sci. Eng.* **2003**, *88*, 186.
(18) Karrai, K.; Grober, R. *Appl. Phys. Lett.* **1995**, *66*, 1842.
(19) Hall, J. E.; Higgins, D. A. *Rev. Sci. Instrum.* **2002**, *73*, 2103.
(20) Moerner, W. E.; Silence, S. *Chem. Rev.* **1994**, *94*, 127.
(21) Mei, E.; Higgins, D. A. *J. Chem. Phys.* **2000**, *112*, 7839.
(22) Higgins, D. A.; Luther, B. J. *J. Chem. Phys.* **2003**, *119*, 3935.
(23) Mei, E.; Higgins, D. A. *Appl. Phys. Lett.* **1999**, *75*, 430.
(24) Santamaria, J. Solvent and Salt Effects. In *Photoinduced Electron Transfer. Part B. Experimental Techniques and Medium Effects*; Fox, M. A., Chanon, M., Eds.; Elsevier: Amsterdam, 1988; p 483.
(25) Kawanishi, Y.; Kitamura, N.; Tazuke, S. *J. Phys. Chem.* **1986**, *90*, 6034.
(26) Feldberg, S. W. *J. Phys. Chem.* **1970**, *74*, 87.
(27) Higgins, D. A.; Liao, X.; Hall, J. E.; Mei, E. *J. Phys. Chem. B* **2001**, *105*, 5874.
(28) Mei, E.; Higgins, D. A. *J. Phys. Chem. A* **1998**, *102*, 7558.